FINITE-BOUNDARY BOWTIE APERTURE ANTENNA FOR TRAPPING NANOPARTICLES

Huapeng Ye[1, *], Haifeng Wang[2], Swee Ping Yeo[1], and Chengwei Qiu[1]

[1]Department of Electrical and Computer Engineering, National University of Singapore, 4 Engineering Drive 3, Singapore 117583, Singapore

[2]Data Storage Institute (DSI), Agency for Science, Technology and Research, DSI Building, 5 Engineering Drive 1, Singapore 117608, Singapore

Abstract—We have found that a single finite-boundary bowtie aperture (FBBA) antenna with gap separation of 10 nm between its tips is capable of confining the electric field to a 18 nm × 18 nm region ($\lambda/39.4$) at 5 nm beneath the gold film and enhancing its near-field intensity by 1,800-fold inside the gap. The FBBA antenna is thus able to provide enhanced trapping potential by virtue of such extraordinarily high (but exponentially decaying) optical near-fields. We have been able to show that 12 nm gold nanoparticles can, in principle, be trapped by the FBBA antenna with 20 nm gap separation; stable trapping is assured where the trapping potential is found to be several times higher than Brownian-motion potential in water. In addition to trapping nanoparticles, this simple but efficient FBBA antenna may find application in near-field optical data storage.

1. INTRODUCTION

Optical antennas convert freely propagating optical radiation into localized energy (and vice versa) [1]. They are of great help in efficiently converting the propagating electromagnetic wave to surface plasmon, thereby overcoming the momentum mismatch between them [2, 3]. Optical antennas have been widely employed as nanosources for higher harmonic light [4, 5], thermal emitters [6],

* Corresponding author: Huapeng Ye (ye.hp.jacky@hotmail.com).

plasmonic sensors [7, 8], and in applications such as photodetection or spontaneous emission efficiency enhancement [9, 10], optical trapping, stacking and sorting [11], and subwavelength field confinement [12].

Traditionally, a hot-spot size in the order of a wavelength can be obtained by means of conventional lens. This kind of hot spot when realized with far-field optics is large and always accompanied by big sidelobes [13]. Far-field optics can be investigated to trap and manipulate micron-sized particle, however, trapping of nanoparticle with far-field optics is constrained by prohibitively high laser power and optical damage at high optical intensity [14]. When the size of nanoparticle is smaller than 100 nm, the trapping force is proportional to the gradient of the electric field intensity. One the other hand, optical forces decrease in accordance with the third power of the nanoparticle size whereas the viscous drag reduces rapidly when the nanoparticle size decreases. Hence, it remains challenge to trap particles of nanoscale dimensions with moderate incident power.

For optical antennas, the surface plasmon arising from the interaction of light with free electrons at a metal-dielectric interface is excited, and the spot size is no longer constrained by the free-space wavelength but by the surface plasma wavelength [15]. They are capable of localizing and enhancing light in their near-field. Generally, there are two kinds of optical antennas — resonant-type antennas (with strong resonance occurring between the boundaries of these antennas and field localization at the boundaries of the antennas) and transmission-type optical antennas (with strong field localization occurring at the center of their transmission apertures) [16]. However, not all the optical antennas could spatially confine the near-field to small area with giant intensity enhancement. The presence of strong cross-polarizations (where the longitudinal field intensity and transverse field intensity are comparable with each other) generally makes the hotspot larger [17]. We should thus focus our investigations on polarization-dependent optical antennas for the purpose of realizing a deep subwavelength hot spot. With the optical near-field consisting mainly of exponentially decaying evanescent waves, we can expect steep intensity gradients to be generated at the near-field [18]. It is possible to exploit this extraordinarily steep gradient for optical trapping, which is widely employed in both biology and physics due to its capability to precisely and noninvasively manipulate micron-sized and nanoscale particles (ranging from atoms and molecules to living cells and viruses [19–22]).

In this paper, we introduce boundary-assisted bowtie-aperture antenna etched on a finite-size gold film (instead of a large-area film). The Lumerical FDTD is employed to study the relationships

between resonant wavelength, near-field enhancement and geometrical parameters of the FBBA antenna. Our simulation results show that the FBBA antenna may be optimized to yield extraordinary enhancement of the localized near-field by more than 1,800 times which is far higher than what can be achieved by a conventional bowtie antenna with the same gap separation. Moreover, we demonstrate the possibility, in principle, of stably trapping 12 nm gold nanoparticles by employing such a FBBA antenna with moderate input power. The optical forces exerted on these nanoparticles are analyzed with dipole approximation theory [18] and offers insight into the mechanism for significant enhancement of trapping potential provided by the FBBA antenna arising from the extraordinarily high (but exponentially decaying) optical near-fields.

2. ANTENNA MODEL AND COMPUTATIONAL APPROACH

Figure 1(a) shows the geometry of the FBBA antenna that is of interest to us. It consists of a rectangular gold film with a bowtie aperture (etched along the longer side of the gold film). This structure is designed to be polarization dependent in the x-direction at normal incidence. To investigate the optical response of this FBBA antenna, we have chosen the FDTD tool from Lumerical FDTD Solutions [23] to perform numerical simulations where the dispersive properties of metals are characterized via multi-coefficient models [24]. In all of these simulations, we adopt a mesh grid of 1 nm by 1 nm by 1 nm and the E-field of the light at normal incidence in the z-direction on the structure is assumed to be linearly polarized along the x-direction as illustrated in Figure 1(a). As the size of the FBBA antenna is finite, source (total-field and scattered-field) with wavelength ranging from 400 nm to 1,200 nm is used in this study.

3. SIMULATION RESULTS AND DISCUSSION

The FBBA antenna's optical response presented in Figure 1(b) shows two resonant wavelengths at 626 nm and 710 nm. We note from the E-field intensity plot in Figure 1(c) that there is a well-confined hot spot at 5 nm beneath the gold film where the light intensity is enhanced by 365 times at the second resonant wavelength. The simulation results for the near-field spot cross sections in the center of the gap region are plotted in Figure 1(d) where it is evident that the full width at half maximum (FWHM) of both x and y-components is around 18 nm ($\lambda/39.4$) Since the FBBA antenna is polarization
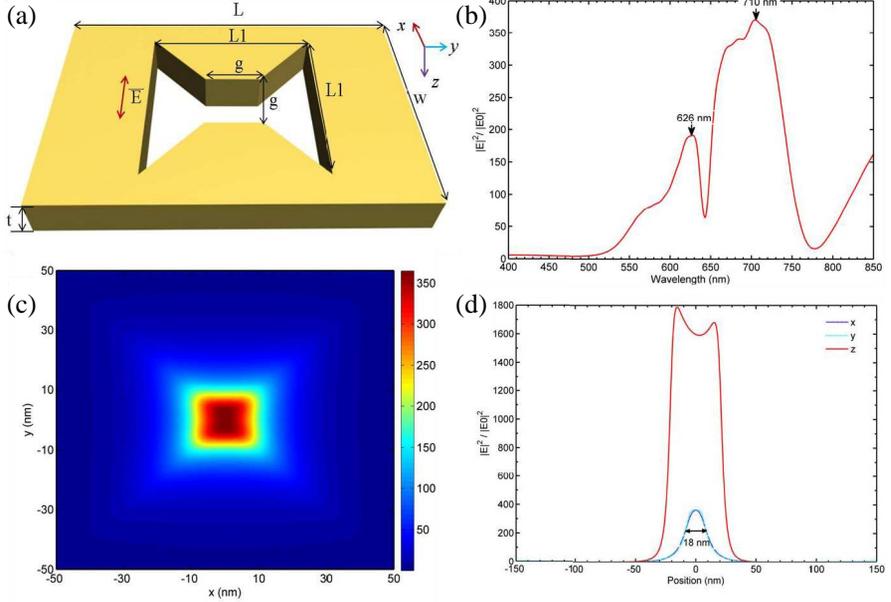
Figure 1. (a) Schematic of FBBA and the incident light polarization configuration. The thickness, width and length of the gold film are denoted with t, w and L, respectively. The bowtie aperture is etched inside the gold film. (b) The optical response of FBBA antenna. (c) The near-field distribution at xy plane, 5 nm beneath the film. (d) FDTD simulated near-field spot cross sections at 5 nm beneath the gold film, where x and y represent field components along x and y directions, respectively. z represents the field enhancement along the light incident direction. The wavelength is 710 nm.

dependent, cross-polarizations [17] are minimized and the hot-spot size is smaller when compared with those obtained by conventional C-aperture [26] and H-shaped nanoantennas. The well-confined hot spot offered by the FBBA antenna may be exploited for high-density near-field optical data storage [25, 26]. Moreover, we infer from the E-field intensity distribution along the light incidence direction (red curve in Figure 1(d)) that the E-field intensity is enhanced by more than 1,600-fold inside the FBBA antenna's gap, which is much bigger than modified bowtie antenna with same gap size [27].

In Figures 2(a) and (c), we vary the width w when plotting the simulation results for resonant wavelength and near-field intensity at 5 nm beneath the gold film (the other parameters are set as $t = 60$ nm,
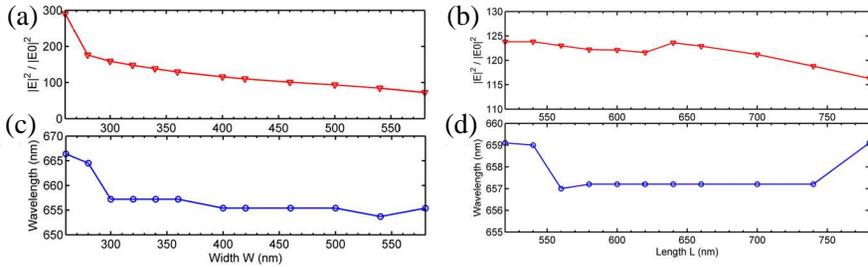
Figure 2. (a) (c) The resonant wavelength and the near-field enhancement at 5 nm beneath the gold film for different film widths. Here, $t = 60$ nm, $g = 20$ nm, $L = 580$ nm and $L_1 = 240$ nm. (b) (d) The resonant wavelength and the near-field enhancement at 5 nm beneath the gold film for different film lengths. Here, $t = 60$ nm, $g = 20$ nm, $w = 320$ nm and $L_1 = 240$ nm.

$g = 20$ nm, $L = 580$ nm and $L_1 = 240$ nm). It can be seen from Figures 2(a) and (c) that the E-field intensity enhancement factor drops from 300-fold to 80-fold when the film width is progressively increased from 260 nm to 580 nm; at the same time, the resonant wavelength shows a slight blue shift of only several nanometers. In Figures 2(b) and (d), we vary instead the length L (the other parameters are set as $t = 60$ nm, $g = 20$ nm, $w = 320$ nm and $L_1 = 240$ nm) and observe that both E-field enhancement factor and resonant wavelength remain almost unchanged (120-fold and 658 nm respectively). Hence, the length of the gold film may be reduced while any reduction of the width needs to accord with the objective resonant wavelength. Under x-polarized incident light, the optical near-fields are strongly enhanced in the gap region due to localized surface plasmon, extra surface plasmon induced from the boundary as well as surface plasmon coupled back because of boundary mismatch between the metal and air. It should furthermore be mentioned that reducing the film size also decreases the metallic loss. This special mechanism makes the near-field intensity much stronger than that obtained by the conventional bowtie aperture antenna [17].

Extending this line of investigation, we proceed to vary the other dimensions when plotting the simulation results for resonant wavelength and near-field intensity at 5 nm beneath the gold film. In Figure 3(a) where we vary the dimension L_1 (with the other parameters set as $t = 60$ nm, $g = 20$ nm, $w = 320$ nm and $L = 580$ nm), the E-field intensity enhancement factor varies from 90-fold to 240-fold and a red shift is observed for the resonant wavelength when the aperture length
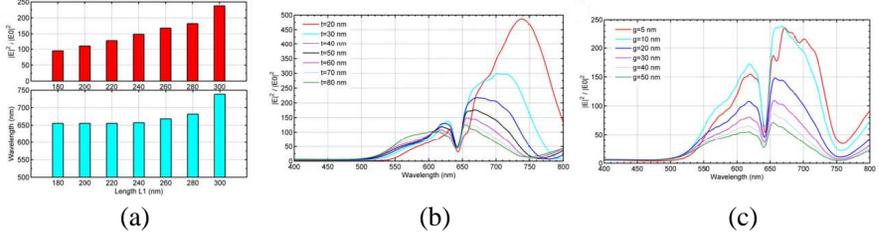
Figure 3. (a) The resonant wavelength and the near-field enhancement at 5 nm beneath the gold film for different aperture lengths. Here, $t = 60$ nm, $g = 20$ nm, $w = 320$ nm and $L = 580$ nm. (b) The resonant wavelength and the near-field enhancement at 5 nm beneath the gold film for different film thicknesses. Here, $L = 580$ nm, $g = 20$ nm, $w = 320$ nm and $L_1 = 240$ nm. (c) The resonant wavelength and the near-field enhancement at 5 nm beneath the gold film for different aperture gaps. Here, $L = 580$ nm, $t = 60$ nm, $w = 320$ nm and $L_1 = 240$ nm.

is progressively increased from 180 nm to 300 nm. In Figure 3(b) where we vary the dimension t (with the other parameters set as $L = 580$ nm, $g = 20$ nm, $w = 320$ nm and $L_1 = 240$ nm), the enhancement at the first resonant wavelength remains almost unchanged but the enhancement factor increases appreciably when the film thickness is progressively decreased from 80 nm to 20 nm. It can be seen that the near-field enhancement at 5 nm beneath the FBBA antenna is bigger than nanoparticles with smaller gap separation [28]. In Figure 3(c), however, where we vary the dimension g (with the other parameters set as $L = 580$ nm, $t = 60$ nm, $w = 320$ nm and $L_1 = 240$ nm), the enhancement factor increases at both resonant wavelengths when the gap width is progressively decreased from 50 nm to 5 nm.

For all of the plots reproduced in Figure 4, we have based our simulations on the same FBBA antenna (with $w = 320$ nm, $L = 580$ nm, $t = 40$ nm, $L_1 = 240$ nm, $g = 20$ nm) which is immersed into water and the nanoparticles are presumed to have been diluted into the liquid. For the plot of near-field intensity along the z-direction in Figure 4(a), the enhancement is extraordinarily high inside the FBBA antenna's gap and near its top and bottom boundaries. Steep gradients are generated when the field intensity decreases sharply at both boundaries. From dipole approximation theory [18], extraordinarily large trapping forces will arise from such steep gradients; if a nanoparticle is placed here, the trapping force exerted on it is proportional to the field intensity gradient and the real
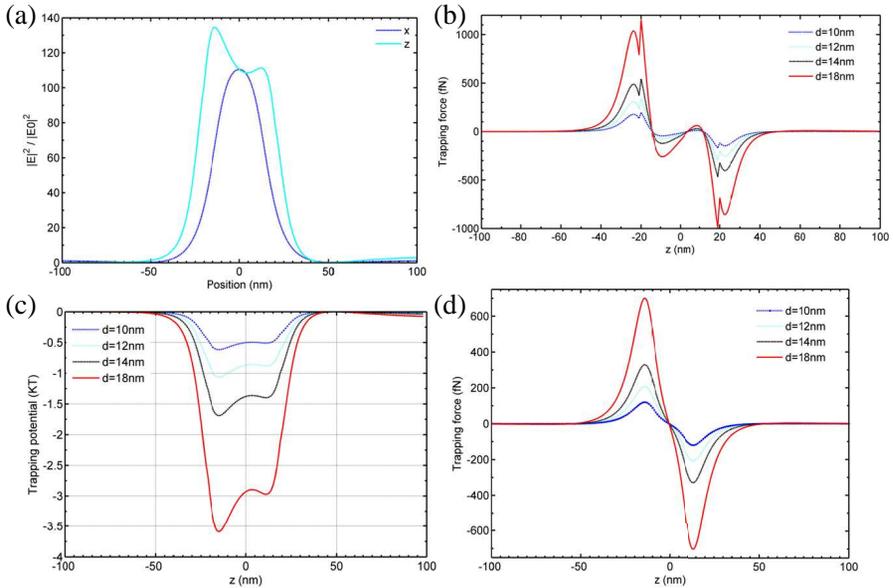
Figure 4. (a) The E-field intensity along z direction through the center of the bowtie aperture. (b) Numerical forces calculated for gold nanoparticles using dipole approximation method based on gradient forces. (c) Trapping potentials normalized to the kinetic energy of Brownian motion in room temperature. The calculations were made from dipole forces, and based on an injected power intensity of $2\,\text{mW}/\mu\text{m}^2$. The kinetic energy of Brownian motion in room temperature is approximately 4.1×10^{-20} J. (d) Optical forces exerted on gold nanoparticles along x direction.

part of its polarizability as can be seen from Equation (1).

$$\langle F \rangle = \left(\alpha'/2 \right) \nabla \left(E \cdot E^* \right) \tag{1}$$

The polarizability of the nanoparticle is defined as [18]

$$\alpha \left(\omega \right) = \alpha' + i\alpha'' = 3\varepsilon_0 V_0 \frac{\varepsilon \left(\omega \right) - \varepsilon_s \left(\omega \right)}{\varepsilon \left(\omega \right) + 2\varepsilon_s \left(\omega \right)} \tag{2}$$

where V_0 and ε are the spherical particle's volume and permittivity respectively, and ε_s is the permittivity of the surrounding medium. It can be seen from these expressions that the optical force exerted on the nanoparticle is proportional to the third power of its diameter. Figure 4(b) presents the plots of the optical force exerted on gold nanoparticles with different diameters, where the electromagnetic

fields are assumed to remain unchanged because the perturbations introduced by such nanoparticles may be regarded as negligible. The permittivity of gold is obtained from experimental data [31], and the positive convention for these optical forces is taken to be the $+z$ direction. It can be observed that the forces are very large near the top and bottom boundaries of the gold film but they fluctuate inside the FBBA antenna's gap. The optical forces at the top and bottom boundaries are in opposite directions, hence giving rise to steep force gradients and extraordinarily deep potential well. The trapping potentials for different nanoparticles derived from $U_z = \int_l F \cdot dz$ [29] are presented in Figure 4(c), which were calculated based on an injected power intensity of $2\,\text{mW}/\mu\text{m}^2$. These trapping potentials have been normalized to the kinetic energy of the nanoparticles' Brownian motion in water at room temperature (with the trapping potential defined to be zero at some infinitely distant location). According to the work reported in [10, 30], the assumption made about the injected power in the calculation is considered low, and safe to the nanoparticles. We infer from the simulation results presented in Figure 4(c) that gold nanoparticles with diameters as small as $12\,\text{nm}$ can be stably trapped inside the gap region [29] (since the trapping potential is slightly higher than the kinetic energy of Brownian motion for $d = 12\,\text{nm}$). The optical forces exerted on different nanoparticles along the x-direction are also presented in Figure 4(d) which indicates that the nanoparticles will be trapped towards the center of the gap under the action of the forces existing there.

4. CONCLUSION

In conclusion, it is found that bowtie-aperture etched on a finite-size gold film is better than its conventional counterpart etched on a large-area gold film in enhancing the localized near-field. We have shown that the E-field intensity is enhanced by more than 1,800 times and the hot-spot size is smaller than $18\,\text{nm}$ by $18\,\text{nm}$ ($\lambda/39.4$), which is suitable for potential application in high-density near-field optical data storage. Furthermore, we have demonstrated the feasibility of trapping $12\,\text{nm}$ gold nanoparticles by means of the FBBA antenna; stable trapping of smaller nanoparticles or molecules is possible provided that the trapping potential is sufficiently large by narrowing the gap separation. Such a FBBA antenna may also find application in on-chip operations for the non-invasive immobilization of metallic nanoparticles.

ACKNOWLEDGMENT

REFERENCES

1. Novotny, L. and N. van Hulst, "Antennas for light," *Nat. Photonics*, Vol. 5, 83–90, 2011.

2. Barnes, W. L., A. Dereux, and T. W. Ebbesen, "Surface plasmon subwavelength optics," *Nature*, Vol. 424, 824–830, 2003.

3. Sun, S., Q. He, S. Xiao, Q. Xu, X. Li, and L. Zhou, "Gradient-index meta-surface as a bridge linking propagating waves and surface waves," *Nat. Materials*, Vol. 11, 426–431, 2012.

4. Navarro-Cia, M. and S. A. Maier, "Broad-band near-infrared plasmonic nanoantennas for higher harmonic generation," *ACS Nano*, Vol. 6, 3537–3544, 2012.

5. Aouani, H., M. Navarro-Cia, M. Rahmani, T. Sidiropoulos, M. Hong, R. Oulton, and S. A. Maier, "Multiresonant broadband optical antennas as efficient tunable nanosources of second harmonic light," *Nano Lett.*, Vol. 12, 4997–5002, 2012.

6. Schuller, J. A., T. Taubner, and M. L. Brongersma, "Optical antenna thermal emitters," *Nat. Photonics*, Vol. 18, 658–661, 2009.

7. Yadipour, R., K. Abbasian, A. Rostami, and Z. D. Koozeh Kanani, "A novel proposal for ultra-high resolution and compact optical displacement sensor based on electromagnetically induced transparency in ring resonator," *Progress In Electromagnetics Research*, Vol. 77, 149–170, 2007.

8. Mortazavi, D., A. Z. Kouzani, and K. C. Vernon, "A resonance tunable and durable LSPR nano-particle sensor: Al_2O_3 capped silver nano-disks," *Progress In Electromagnetics Research*, Vol. 130, 429–446, 2012.

9. Cao, L., J. S. Park, P. Fan, B. Clemens, and M. L. Brongersma, "Resonant germanium nanoantenna photodetectors," *Nano Lett.*, Vol. 10, 1229–1233, 2010.

10. Gao, H., K. Li, F. Kong, H. Xie, and J. Zhao, "Optimizing nano-optical antenna for the enhancement of spontaneous emission," *Progress In Electromagnetics Research*, Vol. 104, 313–331, 2010.

11. Roxworthy, B. J., K. D. Ko, A. Kumar, K. H. Fung, E. K. C. Chow, G. L. Liu, N. X. Fang, and K. C. Toussaint, Jr., "Application of plasmonic bowtie nanoantenna arrays for optical

trapping, stacking, and sorting," *Nano Lett.*, Vol. 12, 796–801, 2012.

12. Pan, L., Y. Park, E. Ulin-Avila, S. Xiong, D. B. Bogy, and X. Zhang, "Maskless plasmonic lithography at 22 nm resolution," *Scientific Reports*, Vol. 1, Article No. 175, 2011, DOI: 10.1038/srep00175.

13. Wang, H., L. Shi, G. Yuan, X. S. Miao, W. Tan, and T. C. Chong, "Subwavelength and super-resolution nondiffraction beam," *Appl. Phys. Lett.*, Vol. 89, 171102, 2006.

14. Ashkin, A., J. M. Dziedzic, and S. Chu, "Observation of a single-beam gradient force optical trap for dielectric particles," *Opt. Lett.*, Vol. 11, 288, 1986.

15. Raether, H., *Surface Plasmons on Smooth and Rough Surfaces and on Gratings*, Springer-Verlag, Berlin Heidelberg, New York, 1988.

16. Wang, H., et al., "Fighting against diffraction: Apodization and near field diffraction structures," *Laser Photonics Rev.*, 1–39, 2011.

17. Wang, H., C. T. Chong, and L. Shi, "Optical antennas and their potential applications to 10 Terabit/in^2 recording," *IEEE: Optical Data Storage Meeting*, 16–18, 2009.

18. Novotny, L. and B. Hecht, *Principle of Nano-optics,* Cambridge University Press, 2006.

19. Chu, S., et al., "Cooling and trapping of neutral atoms," *Phys. Rev. Lett.*, Vol. 57, 314, 1986.

20. Ashkin, A., J. M. Dziedzic, and T. Yamane, "Optical trapping and manipulation of single cells using infrared laser beams," *Nature*, Vol. 330, 769, 1987.

21. Ashkin, A. and J. M. Dziedzic, "Optical trapping and manipulation of viruses and bacteria," *Science*, Vol. 235, 1517, 1987.

22. Yang, A. H. J., M. Lipson, and D. Erickson, "Optical manipulation of nanoparticles and biomolecules in sub-wavelength slot waveguides," *Nature*, Vol. 457, 71, 2009.

23. Lumerical Solutions, Inc., http://www.lumerical.com.

24. Lumerical Solutions, Inc., http://www.lumerical.com/solutions/innovation/fdtd_multicoefficient_ material_modeling.html.

25. Terris, B. D., H. J. Mamin, and D. Rugar, "Nearfield optical data storage," *Appl. Phys. Lett.*, Vol. 68, 141, 1996.

26. Leen, J. B., P. Hansen, Y.-T. Cheng, A. Gibby, and L. Hesselink, "Near-field optical data storage using C-apertures," *Appl. Phys.*

Lett., Vol. 97, 073111, 2010.

27. Da Costa, K. Q. and V. A. Dmitriev, "Bowtie nanoantennas with polynomial sides in the excitation and emission regimes," *Progress In Electromagnetics Research B*, Vol. 32, 57–73, 2011.

28. Kessentini, S. and D. Barchiesi, "Effect of gap shape on the spectral response and field enhancement of dimer-based biosensor," *PIERS Proceedings*, 24–28, Moscow, Russia, Aug. 19–23, 2012.

29. Yang, X., et al., "Optical force in hybrid plasmonic waveguides," *Nano Lett.*, Vol. 11, 321–328, 2011.

30. Cao, T. and M. J. Cryan, "Modeling of optical trapping using double negative index fishnet metamaterials," *Progress In Electromagnetics Research*, Vol. 129, 33–49, 2012.

31. Ordal, M. A., et al., "Optical properties of the metals Al, Co, Cu, Au, Fe, Pb, Ni, Pd, Pt, Ag, Ti, and W in the infrared and far infrared," *Appl. Opt.*, Vol. 22, 1099–1117, 1983.